

Temperature and fluence effects on the evolution of regular surface morphologies on ion-sputtered Si(111)

Ari-David Brown^{1,2} and Jonah Erlebacher²

¹*Department of Physics and Astronomy, Johns Hopkins University, Baltimore, Maryland 21218, USA*

²*Department of Materials Science and Engineering, Johns Hopkins University, Baltimore, Maryland 21218, USA*

(Received 10 January 2005; revised manuscript received 5 May 2005; published 19 August 2005)

Results of a survey of the morphological evolution of the surface of Si(111) are presented for conditions in which regular patterned morphologies are spontaneously created during low energy (250–1200 eV), oblique incidence (60° from normal), Ar⁺ ion beam etching at elevated temperature (500–750 °C). The morphological evolution was found to vary with sputtering time (fluence), ion flux, ion energy, and sample temperature. Experimental regimes in which it is appropriate to analyze ripple evolution in terms of the linear Bradley-Harper theory are identified, through which we find that the activation energy for surface mass transport on ion-bombarded Si(111) is 1.7 ± 0.1 eV, in general agreement with measurements made in other manners. At higher fluence, nonlinear pattern forming effects are observed, including the observation of the formation of three distinct regular morphologies: two types of one-dimensional ripple arrays that differed both in orientation and regularity, and a two-dimensional array consisting of dots, all of which appear in different fluence regimes. All patterns possessed submicron periodicity and nanometer scale amplitudes. In addition, the wavelengths of one-dimensional ripples were often observed to coarsen with fluence, an effect potentially attributable to step-edge dynamics.

DOI: [10.1103/PhysRevB.72.075350](https://doi.org/10.1103/PhysRevB.72.075350)

PACS number(s): 68.35.Bs, 68.37.Ps, 81.10.Aj, 81.15.Np

I. INTRODUCTION

It has long been known that regular arrays of submicron scale features (ripples or dots) sometimes form on metal and semiconductor surfaces etched with keV and sub-keV ions.^{1–4} Physical models of these phenomena have argued that a nonequilibrium pattern forming morphological instability traditionally called sputter rippling leads to such features. Generically, sputter rippling models contain a surface curvature dependent ion-induced etching mechanism⁵ tending to roughen surfaces that competes with thermally activated mechanisms such as surface diffusion^{6,7} or viscous flow⁸ that tend to smoothen surfaces. These etching and smoothening mechanisms operate at different lengthscales over different times, and certain experimental and materials parameters lead to amplification of surface features possessing a “maximally unstable” lengthscale; commonly, this amplification results in a semiperiodic rippled morphology whose wavelength correlates to the maximally unstable lengthscale. Most comparisons between experiment and theory reference a linearized model of etching versus smoothening commonly called Bradley-Harper (BH) theory,⁶ which is valid in the limit of short sputtering times where small slope approximations are valid to describe surface morphologies and the ion range is small compared to surface radii of curvature. Under these conditions, many predictions of the linear BH theory have been experimentally verified, in particular the dependence of ripple orientation on ion beam incidence angle⁹ and the temperature dependence of the ripple wavelength.¹⁰

Most sputter rippling experiments are performed for long enough times that the assumptions of the linear models may no longer be valid, and many interesting and perhaps useful nanoscale surface morphologies have been produced that are

not predicted by linear analytical theory. One intriguing example is the work of Facsko *et al.*¹¹ who have shown that well-organized arrays of dots possessing hexagonal symmetry form on ion-irradiated GaSb surfaces. These dots are of sufficiently large aspect ratio (amplitude/diameter) that the local surface radius of curvature $1/\kappa$ is of order the ion range. Interesting composition dependent differential sputtering may be playing a role in this system, as well as redeposition of sputtered atoms.^{12,13} In single component systems, nonlinear behavior was characterized by Erlebacher *et al.*¹⁴ in the amplitude evolution of 750 eV etched Si(001), in which ripple amplitudes were observed initially to grow exponentially with ion fluence in agreement with predictions of the linear theory, but then were seen to saturate at sufficiently high ion fluence, in variance to the linear theory.

Analytical models of sputter rippling are an area of active interest, and a full description of pattern forming behavior in the nonlinear regime is still lacking. Some important results have been made, however, in particular by Barabasi and co-workers. By accounting for third and fourth order terms in the roughening rate dependence on surface topography (the linear theory only accounts for second order terms⁶), they have extended sputter rippling models into the nonlinear regime^{7,15} and developed a model formally similar to the noisy Kuramoto-Sivanshinsky equation.¹⁶ This model contains ion-beam related terms that lead to (athermal) surface relaxation at sufficiently great surface curvature, and thus explains ripple formation at temperatures for which surface diffusion is not active.

A number of computer simulation studies of sputter rippling,^{17–20} mostly employing Monte Carlo (MC) methods, have attempted to couple the myriad physically relevant microscopic processes that lead to the sputter rippling instability, in a sense offering a solution of the equations of surface

evolution well into the nonlinear regime. For our background purposes here, we focus on the results of three such simulation studies. First, Koponen and co-workers¹⁷ found that ripples formed in the absence of any type of thermally activated surface relaxation using a Monte Carlo (MC) model. These results indicated that ion-induced effective surface diffusion¹⁵ may play an active role in the morphological evolution at low substrate temperature, the effect later explored analytically by Makeev and Barabasi.²¹ Second, simulation studies suggested that not only could amplitudes saturate in the nonlinear regime, but also completely different morphologies (rotated one-dimensional ripple arrays or two-dimensional dot arrays) may also appear at sufficiently high ion fluence.^{18,20} Third, kinetic Monte Carlo (KMC) simulations²⁰ have recently demonstrated that the ripple wavelength may coarsen with ion fluence in contrast to the linear theory,⁶ which predicts that the characteristic periodicity is invariant with fluence. The KMC model is relevant to our discussion of step-edge dynamics, below.

Here we present results from an experimental survey of the morphological evolution of the surface of Si(111) for conditions in which regular patterned morphologies are spontaneously created during keV and sub-keV energy (250–1200 eV), oblique incidence (60° from normal), Ar⁺ ion beam etching at elevated temperature (500–750 °C), and the further influence on morphological evolution by ion fluence and ion flux. A significant number of observations were made that correspond to effects not associated with linear BH theory, including the formation of three regular but transient morphologies: two types of one-dimensional ripple arrays that differed both in orientation and regularity (parallel ripples with wave vector oriented parallel to the projected ion beam, i.e., ripples oriented perpendicular to the projected beam direction, and perpendicular ripples with wave vector oriented perpendicular to the projected beam direction, i.e., ripples oriented parallel to the projected beam direction) and a two-dimensional array consisting of a superposition of parallel and perpendicular mode ripples. Also, one-dimensional ripples were observed to coarsen, in which the apparent ripple wave vector sputtering time functional dependence was best described by an offset exponential decay.

The discussion of our results focuses on two issues. (a) *Does the linear BH theory describe our results at any time?* This question arises because we observe both the wavelength of each ripple mode to coarsen with fluence and to saturate in amplitude, effects associated with nonlinear behavior. We show that analysis of ripple evolution at very low fluence yields results consistent with predictions of the linear BH model, and also provides the first direct experimental measurement of the roughening and relaxation factors in the linear model. (b) *What causes ripple wavelength coarsening?* The basis of amplitude saturation has been discussed in the literature, and includes effects such as ion induced effective surface diffusion²¹ and step-step interactions leading to terrace pinch-off at the peaks of growing ripples, in turn leading to amplitude saturation.¹⁴ Castro and co-workers¹³ have made the analytical prediction that the characteristic length of the surface morphology follows a power law dependence on time (fluence), a functional form that accurately describes coarsening of InP sputter dots²² formed during oblique inci-

dence sputtering of a rotating sample. However, it does not explain well the ripple coarsening on Si(111) that we report here, which, as we discuss below, does not follow a power law. We believe that the inability of Castro *et al.*'s theory to predict the details of coarsening on Si(111) ripples might be attributed, in part, by their assumption that the microstructure of the sputtered surface is amorphous. In the experiments reported here, the substrate temperature is sufficiently high that recrystallization occurs faster than etching, so that our surfaces remain crystalline. To explain our results, we show that a simple model incorporating step-step dynamics upon a crystalline surface will lead to ripple coarsening, in qualitative agreement with our results for Si(111).

The paper is structured as follows: in Sec. II, an overview of linear BH theory is presented as a theoretical foundation to which much of our data will be compared. In Secs. III and IV, respectively, we describe the experimental details and our results. Our discussion, Sec. V contains two sections. In Sec. V A, we discuss small fluence results and interpret these results within the linear BH theory. In Sec. V B, we discuss possible origins for ripple coarsening. Finally, Sec. VI contains conclusions.

II. BRADLEY-HARPER THEORY OF SPUTTER RIPPLING

Bradley-Harper theory (BH)⁶ predicts the functional dependence of the ripple wavelength with substrate temperature, ion energy, and ion flux and the temporal evolution of ion sputtered surfaces for short sputtering times. The model sets up a competition between ion-induced surface roughening as described by Sigmund's model of a local surface curvature-dependent sputtering yield,⁵ and surface smoothing due to surface diffusion on a surface above its roughening temperature.²³

BH use perturbation analysis in the small slope limit (for which the surface curvature $\kappa = -(\partial^2 h / \partial x^2) / [1 + (\partial h / \partial x)^2]^{3/2} \approx -\partial^2 h / \partial x^2$) to derive the following expression for the surface amplitude $h(x, y, t)$ evolution:

$$\frac{\partial h}{\partial t} = -v_0(\theta) + v'_0(\theta) \frac{\partial h}{\partial x} + fa\Omega Y_0(\theta) \left[\Gamma_1(\theta) \frac{\partial^2 h}{\partial x^2} + \Gamma_2(\theta) \frac{\partial^2 h}{\partial y^2} \right] - B\nabla^2 \nabla^2 h. \quad (1)$$

The first term on the right-hand side of Eq. (1) is the erosion rate of an unperturbed surface at an angle θ between the surface normal and incident ion direction (oriented along the x direction). The second term and third terms describe ion-induced roughening; $v'_0(\theta)$ is the velocity at which ripples travel due to anisotropic etching of the front and rear surfaces of a perturbation with wave vector in x , f is the ion flux, a is the ion range, Ω is the atomic volume, $Y_0(\theta)$ is the sputtering yield of a flat surface with slope θ , and the Γ prefactors to the principle curvatures in the small slope limit account for the fact that the sputtering yield of a ripple valley is larger than that for a ripple crest. The curvature effect on sputtering is athermal and anisotropic when the sample is being ion etched at oblique incidence, as in our case here.

Surface smoothing by surface diffusion is accounted for by the final term on the right-hand side of Eq. (1). The

smoothing prefactors are usually taken to be of the classical form describing isotropic surface diffusion above the surface roughening transition temperature:

$$B = \frac{D_s \nu \gamma \Omega^2}{k_B T} \quad (2)$$

This factor depends upon the surface diffusivity D_s (which has an Arrhenius temperature dependence), the surface energy γ , Boltzmann's constant k_B , the substrate temperature T , and the concentration ν of mobile species. Assuming that the mobile species are point defects such as adatoms or terrace vacancies, the steady-state value of ν may be due to a balance between their creation rate due the ion beam (an athermal process) and their annihilation rate due to direct ion impingement, or diffusion to traps such as other defects or step edges.¹⁰ However, in the absence of information regarding the particular nature of the surface diffusers, one needs to consider also the possibility that the concentration of mobile species maintains thermal equilibrium with the surface. In this case, ν is also a thermally activated quantity, and the temperature dependence of B may be written in the form

$$B = \frac{B_0}{k_B T} e^{-E/k_B T}, \quad (3)$$

where $B_0 = D_0 \nu_0 \gamma \Omega^2$. In this equation, we have separated the temperature dependence of $D_s = D_0 e^{-E_d/k_B T}$ and $\nu = \nu_0 e^{-E_f/k_B T}$. The effective activation energy for mass transport during sputter patterning for the case of thermalized diffusers is thus the sum of a migration and formation energy, $E = E_d + E_f$. However, for an athermal concentration of diffusers ν , $E = E_d$. Thus our experimental measurement of an activation energy for surface diffusion under ion bombardment may be considered an upper bound for the migration energy.

A linear stability analysis of surface evolution using Eq. (1) in two-dimensional Fourier space results in a growing ripple morphology that may be expressed as a linear combination of ripple modes growing with wave vector in x , parallel to the projected ion beam direction ("parallel ripples") and ripple modes growing with wave vector in y , perpendicular to the projected ion beam direction ("perpendicular ripples"). Because of the term containing $v'_0(\theta) \partial h / \partial x$ in Eq. (1), parallel mode ripples are traveling wave modes. The amplitude of each Fourier mode $h_q(t)$ in either orientation, with wavelength $\lambda = 2\pi/q$, grows independently at short times according to

$$h_q(t) = h_q(0) e^{R_q t}, \quad (4)$$

where the amplification factor R_q is related to lengthscale-dependent roughening and relaxation factors and is time invariant. This quantity is usually expressed as

$$R_q = -Aq^2 - Bq^4, \quad (5)$$

where

$$A = fa\Omega Y_0(\theta) \Gamma(\theta). \quad (6)$$

For perpendicular mode ripples, Γ_2 is used; for parallel mode ripples, Γ_1 is used. For all experimental conditions (e.g., ion beam incidence angle) $\Gamma_2 < 0$ indicating that perpendicular

mode ripples are always in principle activated (i.e., $-Aq^2 > 0$). At sufficiently glancing incidence below a critical angle θ_{crit} , $\Gamma_1 < \Gamma_2$. For these conditions, the surface modes with the fastest growing amplitude are parallel mode ripples, and of these, the mode with the fastest growing amplitude is expected to dominate the morphological evolution. In either case, the analysis predicts the existence of a characteristic wave mode q^* , that grows faster than all of the other modes:

$$q^* = \sqrt{\frac{-A}{2B}}. \quad (7)$$

The particular value of A to use depends on the minimum of (Γ_1, Γ_2) . If the temperature and flux dependence of the various terms contained within A and B are known, it is straightforward to obtain the functional dependence of the characteristic wavelength upon these various experimentally controllable parameters.¹⁰

III. EXPERIMENT

Sputter rippled samples were made inside of an UHV chamber with a base pressure of 6.0×10^{-11} Torr on 3 in. Si(111) wafers (n -type, As-doped, 0.002–0.020 Ω cm). Sample temperature was controlled using a pyrolytic boron nitride/graphite filament backside radiant heater and monitored using a thermocouple spring-loaded to the rear of the sample and an infrared thermometer that probed the sample surface; the samples were maintained at temperatures between 500 and 750 °C. Sample blackbody spectra were also collected using light scattering spectroscopy (discussed below). All referenced sample temperatures were in the center of the sample wafer. A collimated and neutralized Ar⁺ ion beam from a Kaufmann ion source was directed 60° from the surface normal and was oriented parallel to the $[1\bar{1}0]$ direction on the silicon surface. The samples could be rotated azimuthally to within a precision of 8.8 arcsec with our homebuilt sample manipulator. In this study we varied the ion energy ε between 250 and 1200 eV and ion flux between 0.38 and 3.0 mA/cm². The temperatures at which these experiments were performed are high enough that recrystallization always occurs much faster than amorphization during individual ion impacts.²⁴

Quantitative information regarding the ripple amplitude and periodicity, in addition to the sample morphology, was obtained using *ex situ* atomic force microscopy (AFM) and *in situ* UV light scattering spectroscopy (LiSSp).²⁵ Our LiSSp apparatus consists of a broadband 300 W Xe source that is used to illuminate an approximately 10 mm² region in the sample center. A spectrum of nonspecular scattered light is then collected at a fixed angle by a charge-coupled device array. Peaks in this spectrum are due to surface features with sufficient periodicity to satisfy the Bragg condition. The details of LiSSp are discussed elsewhere;²⁵ in short, a LiSSp spectrum is proportional to the morphological power spectrum of the surface,²⁶ and thus data may be represented by plotting the square of the Fourier component of the surface morphology versus Fourier component wave number. We obtain a proportional measure of the magnitude of the Fourier

decomposition of the surface morphology h_q vs wave number q by examining the square root of the LiSSp spectrum. In our apparatus geometry, we are able to use LiSSp to probe feature periodicities between 450 nm and 1.1 μm .

In this experiment, LiSSp spectra were collected at time intervals during sputtering runs that typically lasted more than 5 h. A typical collection time was of order 10 s. It was necessary to turn off the ion beam while obtaining spectra to avoid interference effects from the Ar^+ plasma, thus creating the possibility of surface relaxation during the short intervals in which LiSSp spectra were collected. However, multiple comparisons between samples analyzed only by *ex situ* AFM and identical samples also probed by LiSSp indicated that such an effect, if present, was negligible. The evolution of both parallel and perpendicular modes was accomplished by rotating the sample 90° during a collection period. *Ex situ* AFM was used to confirm morphological information obtained by LiSSp. In addition, AFM was used to determine sample feature sizes that were outside of the LiSSp detection range.

The lack of surface relaxation during collection of LiSSp spectra suggested that surface relaxation does not occur on the experimental time scale while the beam was turned off. To examine this further, we annealed a number of our samples at 750°C for 48 h and did not observe any measurable difference in the surface amplitude. This observation suggests that the concentration of species participating in surface diffusion during the evolution of sputter ripple patterns is to a great degree controlled by athermal creation mechanisms due to the ion beam.

IV. RESULTS

Our results consist of LiSSp spectra and AFM micrographs which are used to describe the morphological evolution of ion sputtered Si(111). Initially we present general features of ripple evolution at different temperatures and fluence, and then describe details of coarsening behavior. We then present results of studies in which the ion flux and ion energy were varied.

A. General morphological behavior vs temperature and fluence

The AFM micrographs shown in Fig. 1 are representative of the morphological evolution of Si(111) sputter ripples. Sputtering conditions for this sample were $T=637^\circ\text{C}$, $\epsilon=500\text{ eV}$, $f=0.75\text{ mA/cm}^2$, and micrographs were taken for samples sputtered for $t=1800$, 3600, and 10 260 s, respectively. For low ion fluence, parallel ripples form; at higher fluence, perpendicular ripples begin to appear superimposed on the parallel ripples leading to the formation of a two-dimensional array of dots with quasirectangular symmetry. After very long sputtering time, the parallel ripples disappear, leaving only perpendicular ripples, and at even longer times, the surface becomes randomly rough. For this ion flux and energy, this double morphological transition was seen on samples with temperatures between 630 and 700°C . This range is limited because parallel ripples disappear very

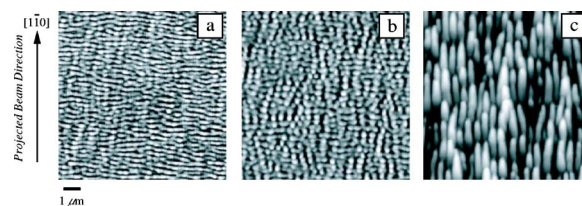


FIG. 1. (Color online) AFM topographs showing the morphological progression of ion sputtered Si(111) at $T=637^\circ\text{C}$ and $f=0.75\text{ mA/cm}^2$. (a) After short sputtering time, $t=1800\text{ s}$, parallel ripples form; (b) after longer sputtering time, $t=3600\text{ s}$, perpendicular ripples appear leading to a two-dimensional morphology. At much larger ion fluence, $t=10\,260\text{ s}$, the parallel ripples vanish leaving a new one-dimensional morphology, shown in (c). The feature periodicity and distance between the ripple peak to valley for each case are (a) 300 and 1.5 nm, (b) 393 nm (parallel)/600 nm (perpendicular) and 3.75 nm, and (c) ~ 650 and ~ 35 nm, respectively.

quickly for $T < 630^\circ\text{C}$ and perpendicular ripples grow very slowly when the sample temperature is above 700°C . Thus, for all samples discussed that were formed at temperatures greater than 700°C ($f=0.75\text{ mA/cm}^2$), we only observed parallel mode ripples. In addition, because of limitations in the LiSSp detection range, evolution of perpendicular mode ripples was followed primarily at low temperature ($600\text{--}685^\circ\text{C}$) while the evolution of parallel mode ripples was followed primarily at high temperature ($T > 700^\circ\text{C}$).

Visual inspection suggests that the two one-dimensional modes are fundamentally different; parallel ripples are much more regular and possess a much smaller amplitude than their perpendicular counterparts. This observation is confirmed by representative LiSSp spectra shown in Fig. 2. The spectrum corresponding to the parallel mode rippled sample is much more sharply peaked (smaller width at half-max) and is much less intense than that of the perpendicular mode sample, indicating that the feature size distribution is much more mono-disperse in the former case. The LiSSp spectrum also confirms an AFM observation that, while more regular, the amplitude of parallel mode ripples is much smaller than that of the perpendicular mode ripples.²⁷ We reiterate that this phenomena involving ripple formation followed by dot and, finally, rotated ripple formation during oblique incidence ion sputtering has been observed previously in computer simulations.^{18,20} Although there may be some evidence that this effect has been seen in sputter rippled Cu(001),²⁸ the effect really is quite dramatic in Si(111).

B. Coarsening of one-dimensional ripple modes

Apart from morphological transitions, another ubiquitous feature of the evolution of ripples on Si(111) is ripple coarsening as the sputtering time increases. Regardless of ripple orientation, coarsening was observed; that is, while parallel mode ripples dominated the morphology, they coarsened, and while perpendicular mode ripples dominated the morphology, they coarsened. The effect is illustrated in Fig. 3, which shows a series of LiSSp spectra obtained from parallel and perpendicular mode rippled samples. While measur-

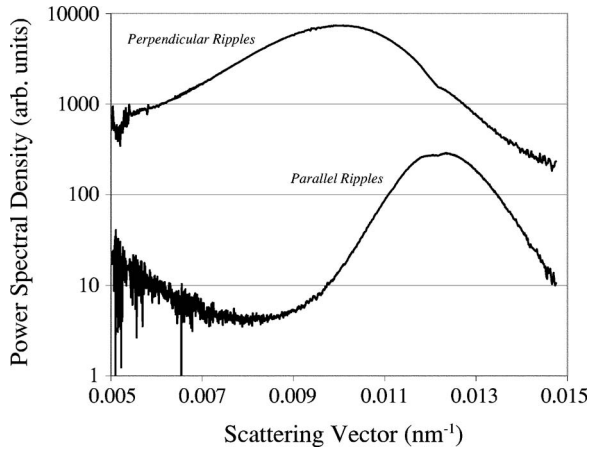


FIG. 2. Representative LiSSp spectra of samples where the ripple morphologies are most highly regular (i.e., the spectra are most intense and sharply peaked). The noise in the spectra seen for $q < 0.007 \text{ nm}^{-1}$ is due to the spectrometer detection limits. The perpendicular mode spectrum was taken of a sample sputtered at $T = 644 \text{ }^\circ\text{C}$ for 6840 s and the parallel spectrum was taken after $t = 57\,600 \text{ s}$ at $717 \text{ }^\circ\text{C}$; for both, the ion flux $f = 0.75 \text{ mA/cm}^2$. Parallel mode ripples are seen to be more organized as indicated by a sharper peak width whereas perpendicular mode ripples have greater amplitude.

able coarsening occurs after short periods of ion etching ($\sim 600 \text{ s}$), feature coarsening is actually a relatively minor effect considering the high flux and fluence; we find that the parallel and perpendicular ripple wavelength increases by at most a factor of 1.32 and 1.78, respectively, for fluence of order $1.6 \times 10^{20} \text{ ions/cm}^2$.

Close inspection of the apparent characteristic scattering vector q_{app} , defined as the position in q -space where the power spectrum is peaked, reveals that for both parallel and perpendicular mode ripples, q_{app} decays exponentially with fluence (we make a distinction between the experimentally derived apparent wave vector q_{app} and the maximally unstable wave vector q^* as predicted by theory). Figure 4 shows representative data for q_{app} vs time for different temperatures. We note that the data are best fit (with fitting parameters y_0, Λ, τ) by an offset exponential decay, an empirical fit of the form

$$q_{app}(t) = y_0 + \Lambda e^{-t/\tau}. \quad (8)$$

The linear BH theory does not contain a prediction of such coarsening. However, we can connect to the linear behavior by considering the $t \rightarrow 0$ limit of this empirical form. At $t = 0$, $q_{app}(0) = y_0 + \Lambda$ is characteristic of ripple evolution at a particular temperature, i.e., it should be equivalent to q^* in Eq. (7). Our data for $q_{app}(0)$ for parallel mode ripples shows a clear decrease in $q_{app}(0)$ with temperature for $T > 700 \text{ }^\circ\text{C}$, as shown in Fig. 5. For perpendicular mode ripples $q_{app}(0)$ appears, within experimental resolution, nearly constant with temperature.

Additional information obtained from LiSSp spectra can be used to highlight the differences between parallel and perpendicular mode sputter etched features. Because the square

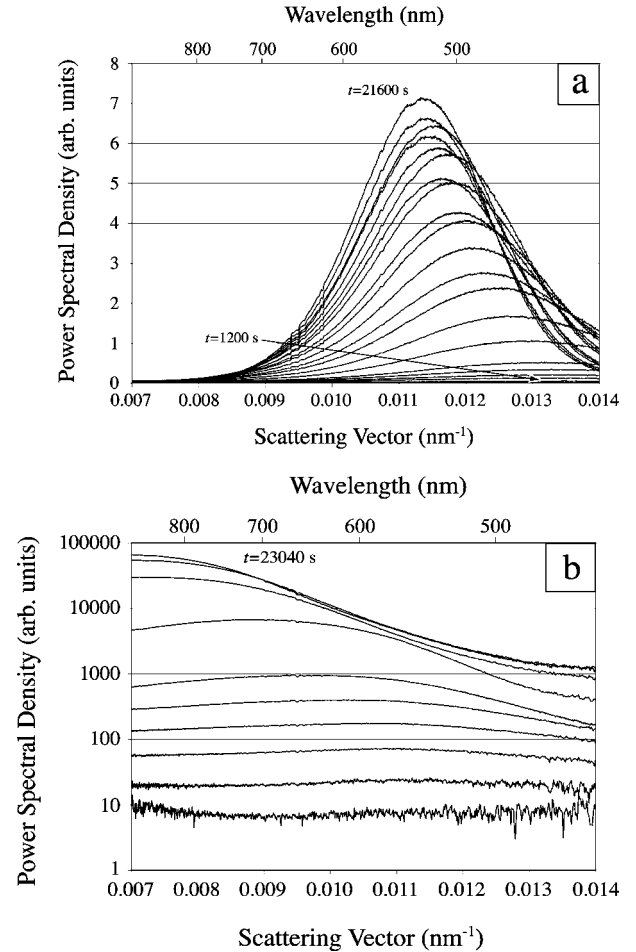


FIG. 3. LiSSp spectra showing the morphological evolution of ripples: (a) parallel mode ripples at $T = 733 \text{ }^\circ\text{C}$ and (b) perpendicular mode ripples at $T = 629 \text{ }^\circ\text{C}$. Note that the power spectral density of the surface morphology increases with time and becomes more sharply peaked, indicating ripple formation. Also note the peak shift toward lower scattering vector indicating ripple coarsening.

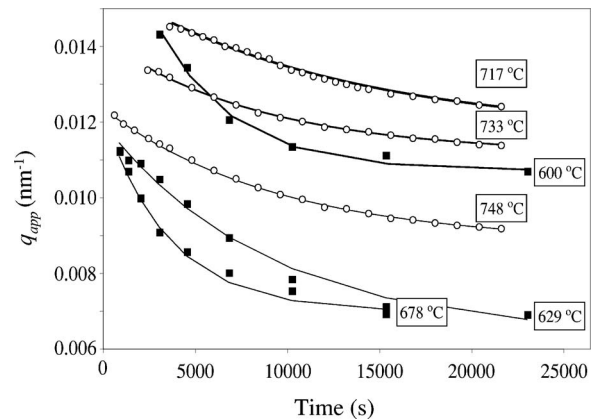


FIG. 4. Apparent wave vector q_{app} vs time t for parallel ripples (open circles) and perpendicular ripples (closed squares) at various sample temperatures. Lines: fits to offset exponential decay functional form [Eq. (8)].

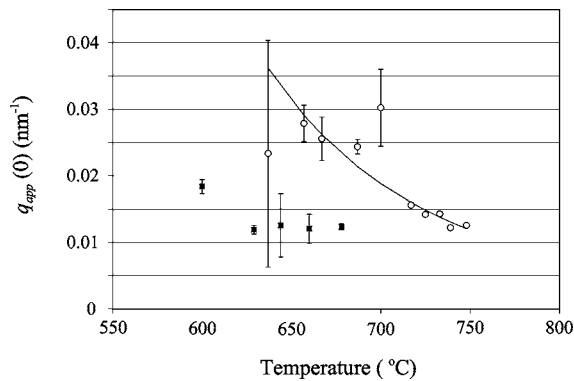


FIG. 5. (Color online) Apparent ripple wave vector $q_{app}(0)$ vs T for parallel ripples (open circles) and perpendicular ripples (closed squares). Line: fit to the linear BH form (Ref. 6).

root of power spectral density approximately scales linearly with corrugation amplitude,²⁹ we find that the ripple aspect ratio ($=h/\lambda_{app}$) stays roughly constant during growth for parallel mode ripples. However, for perpendicular mode ripples, the aspect ratio first rises quickly but then decreases as kinetic roughening becomes more prominent.

C. Effect of flux on ripple morphology

For the particular value of $f=0.75$ mA/cm² and sample temperatures above approximately 685 °C, parallel ripples were never seen to disappear (at any fluence) and be replaced by perpendicular mode ripples. That is, the morphological transition and transient observation of two-dimensional ripples was not observed. However, by increasing f , we were able to increase the cutoff temperature above which perpendicular mode ripples did not form. In general, our results indicate that higher ion flux suppresses the parallel ripple mode and promotes the perpendicular ripple mode formation. This behavior is clarified using two different types of data, as shown in Fig. 6. The first type consists of a series of LiSSp spectra (a) of ripples produced at $T=644$ °C and ion fluence of 3.2×10^{19} ions/cm². For $f=0.60$ mA/cm², the parallel mode spectrum is peaked at 0.0111 nm⁻¹; however, for $f=0.75$ mA/cm², no parallel mode peak is detected. The second example is shown in two AFM micrographs of patterns formed at $T=717$ °C and fluence of 7.2×10^{19} ions/cm². Two distinct morphologies are created; perpendicular mode ripples are clearly forming in the sample bombarded with higher flux.

The functional dependence of wavelength with ion flux has been studied on low energy Ar⁺-etched Si(001),¹⁰ where it was found that $\lambda \sim f^{-0.5}$. In that system, only perpendicular mode ripples form, and they possess no fluence dependence.¹⁰ For Si(111), it was not initially clear how such a study be undertaken because the sputter ripple periodicity varied with ion fluence. Our approach was to analyze the morphological behavior by examining the wavelength as a function of flux at fixed ion fluence. In two experiments, we found that for parallel mode ripples the feature wavelength at fixed fluence appear to be independent of the ion flux. For a sample temperature of $T=717$ °C, for a fluence of 9.6

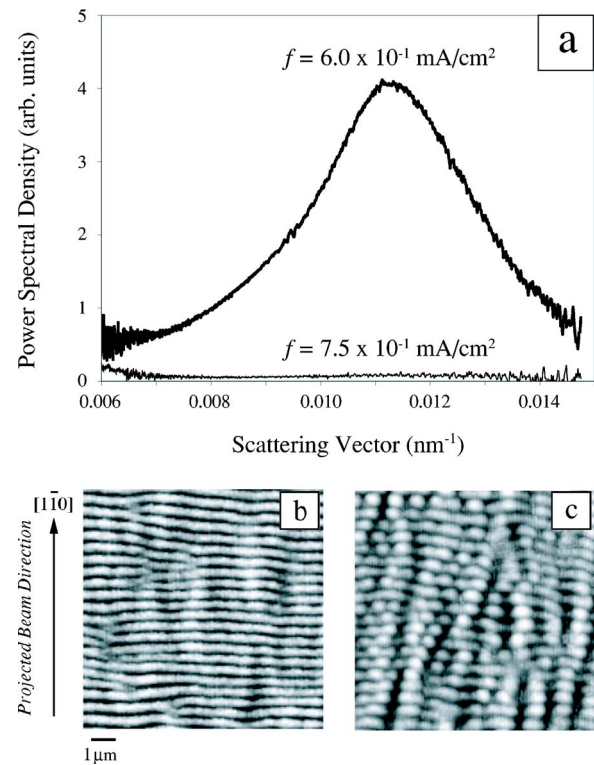


FIG. 6. (Color online) Examples of ripple annihilation and creation due to increased ion flux. (a) LiSSp spectra of parallel mode features at 644 °C and 3.2×10^{19} ions/cm² where low f is 0.60 mA/cm² and high $f=0.75$ mA/cm². (b) and (c): AFM images of patterns formed with low ($=0.75$ mA/cm²) flux (b) and high ($=0.98$ mA/cm²) flux (c). Note the appearance of perpendicular ripples in (c).

$\times 10^{19}$ ions/cm², we observed average ripple wavelength of 480 nm both for $f=0.75$ mA/cm² and for $f=0.98$ mA/cm². At the same temperature, for a fluence of 2.1×10^{20} ions/cm², the wavelength was found to be 640 nm both for $f=0.75$ mA/cm² and for $f=1.7$ mA/cm², respectively. The wavelength of perpendicular mode ripples at fixed fluence exhibited small stochastic variation with f , for flux ranging between 0.53 and 1.5 mA/cm².

D. Effect of ion energy on ripple morphology

Rippling morphologies were also examined by varying ion energy ϵ at fixed temperature; differing behavior was seen for each ripple mode. A series of AFM micrographs of parallel mode sputter ripples formed to an ion fluence of 7.2×10^{19} ions/cm² at $T=717$ °C are shown in Fig. 7. As the ion energy is increased from 250 to 1200 eV, there is a dramatic increase in the regularity of the ripple pattern, and also a significant decrease in the ripple amplitude and wavelength. We note that this decrease in amplitude with ϵ was also observed on Si(001) sputter ripples.³⁰ The ripple wavelength was found to scale with energy as $\lambda \sim \epsilon^{-\alpha}$, where a least-squares fit of the wavelengths corresponding to the micrographs shown in Fig. 7 yielded $\alpha=0.45 \pm 0.04$. In contrast, no clear trend was observed for perpendicular mode ripples, which we probed for at $T=657$ °C, 3.2×10^{19} ions/cm². Ini-

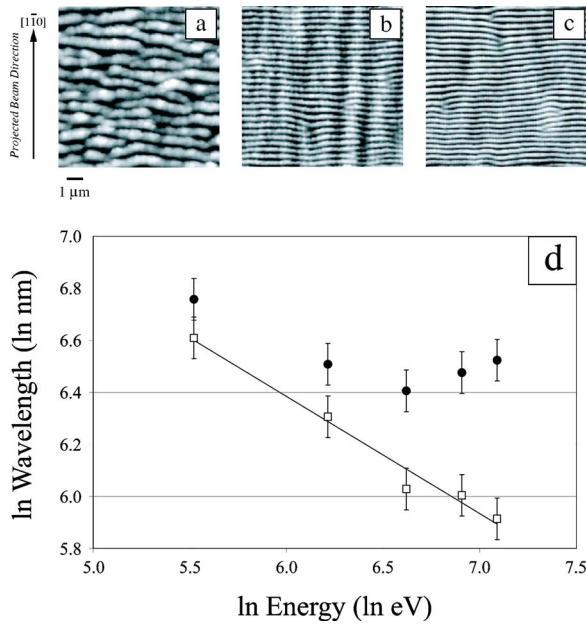


FIG. 7. (Color online) Ripple morphologies for different ion energy ε : (a) 250 eV, (b) 750 eV, and (c) 1200 eV. The wavelength (amplitude) is 740 nm (12 nm), 415 nm (~ 4 nm), and 350 nm (~ 4 nm), respectively. Sample sputtering conditions were $T = 717$ °C, fluence= 7.2×10^{19} ions/cm². (d) log-log plot of ripple wavelength vs ion energy for parallel ripples (squares) and perpendicular ripples (dots). Perpendicular mode ripples were formed at $T = 657$ °C, fluence= 3.2×10^{19} ions/cm², and the line corresponds to $\lambda = 8845.34\varepsilon^{-0.45}$.

tially, the wavelength was found to decrease (with $\alpha = 0.26 \pm 0.06$) and then increase with ε ; the minimum was located at $\varepsilon = 1000$ eV, illustrated in Fig. 7(d).

V. DISCUSSION

A. Analysis of surface morphological evolution in the linear regime

Generally, we found that for low ion fluence ($< 1.1 \times 10^{19}$ ions/cm²), the amplitude of a particular surface morphological wave mode h_q could be interpreted initially to increase exponentially with amplification factor R_q . The typical time evolution of a surface morphology Fourier component is illustrated in Fig. 8, and exponential increases in amplitude were observed for both parallel and perpendicular mode ripples. The linear BH theory⁶ indeed predicts that there should be an exponential increase in the amplitude of each wave mode before nonlinearities begin to dominate morphological evolution. For each wave mode, we observe a crossover time t_{\max} , after which h_q saturates or even decreases with fluence.

By close analysis of the evolution of wave modes in the LiSSp data, we found R_q for each surface mode q . First, we smoothed our LiSSp spectra by performing a 3-point boxcar average in order to minimize stochastic noise in the data. Second, we separated for further analysis from our data $h_q(t)$ for all sputtering time less than or equal to t_{\max} (here t_{\max} is always greater than 1800 s when using a flux of

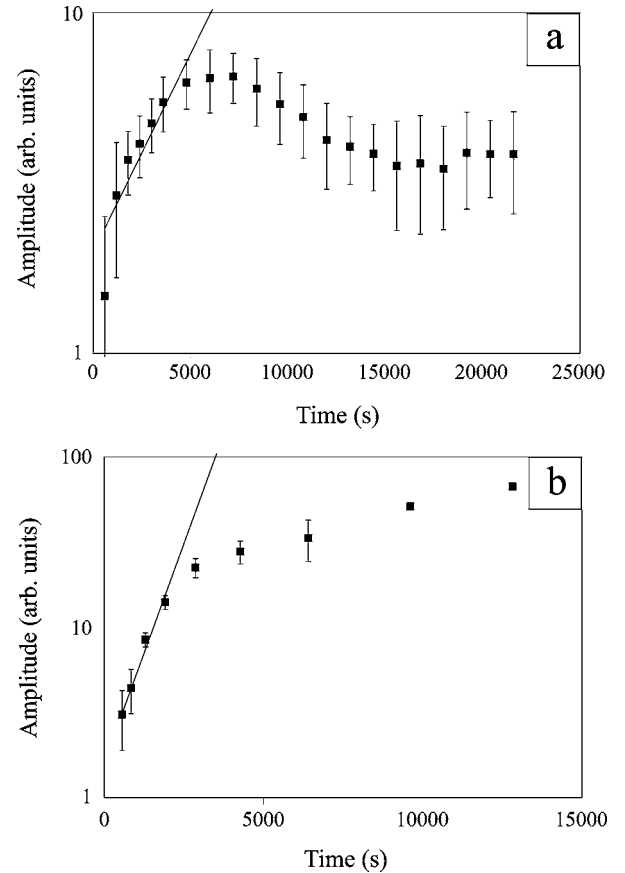


FIG. 8. Typical time evolution of surface morphology Fourier components, $h_q(t)$ for $q = 0.01257$ nm⁻¹ (ion flux= 0.75 mA/cm²): (a) $T = 739$ °C and (b) $T = 644$ °C. Fitted lines correspond to early exponential growth prior to ripple saturation. Amplitude error bars were obtained from the corresponding LiSSp spectrum as the rms deviation from the mean of a 3-point boxcar average of data surrounding q .

0.75 mA/cm² and can sometimes be as large as 7200 s). Third, we performed a linear regression of $\ln(h_q(t))$ versus t for each q ; R_q is the slope of this line. Representative examples of the results of this procedure for parallel and perpendicular mode ripples are shown in Fig. 8.

Analysis of the spectrum of R_q should provide a good test of the linear BH theory. Figure 9 shows a representative example of R_q vs q , which shares some general characteristics found in all of our samples and to the predictions of BH theory: (1) The curve is peaked, and (2) the position of this peak is comparable to a characteristic corrugation wave vector directly observed using either LiSSp or AFM. Fitting Eq. (5) to the spectrum of R_q vs q data to obtain quantitative values for the roughening and relaxation factors A and B did not work unless the spectrum was shifted along the R_q axis, i.e., a good fit could only be made to the form $R_q = -Aq^2 - Bq^4 + C$. We are unable to ascribe either an intrinsic physical interpretation or a systematic experimental parameter to account for the presence of the offset parameter C . One possible origin, however, is the presence of long-range weak correlations, perhaps due to strain fields, shadowing, etc. Such long range, weak effects are known to manifest them-

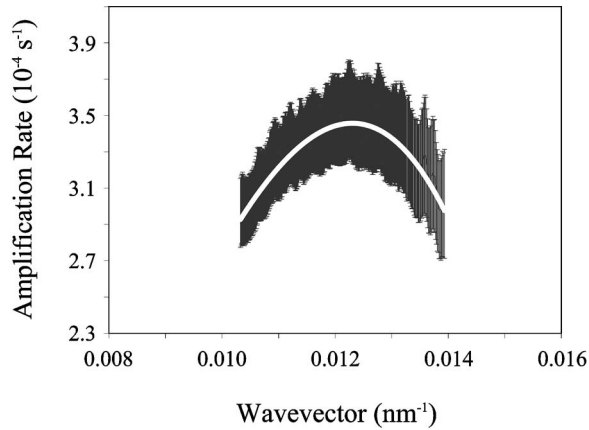


FIG. 9. Example of the extracted ripple amplification rate R_q vs wave vector q for parallel mode sputter ripples formed at 733 °C. The white line is a fit to the form predicted by BH theory (Ref. 6) [cf. Eq. (5)], and A , B , and C were found to equal $-8.00 \times 10^{-14} \text{ cm}^2/\text{s}$, $2.64 \times 10^{-24} \text{ cm}^4/\text{s}$, and $-2.60 \times 10^{-4} \text{ s}^{-1}$, respectively.

selves as a constant shift in the response spectrum, as we see here, at least for small enough q .³¹ We have performed some numerical analysis of such effects, and our preliminary conclusions, to be reported later, are that such effects do not interfere with the functional dependence of A , B on experimental parameters as presented above.

The values we find for the roughening and relaxation parameters A and B by fitting reduced LiSSp data to Eq. (5) are reasonable, even considering that we do not know the origin of the offset value C . As an example, for the data shown in Fig. 9, values of A and B were found to equal $-8.00 \times 10^{-14} \text{ cm}^2/\text{s}$ and $2.64 \times 10^{-24} \text{ cm}^4/\text{s}$, respectively. These values are near to estimates made using fundamental values plugged into Eqs. (2) and (6). For instance, using $Y = 1.92 \text{ atoms/ion}$,³² $a = 2.8 \text{ nm}$,³³ and $\Gamma_1 = -9.88 \times 10^{-2}$,^{6,33} we estimate that A is $-4.98 \times 10^{-15} \text{ cm}^2/\text{s}$. Considering that this estimate contains large uncertainties, primarily in the range a (for which we used SRIM) and in Γ_1 (which can change by an order of magnitude or more when the ratio between the ion range and straggle is varied), the comparison is promising.

Comparisons of the experimental value for B to the theoretically predicted ones rely on knowledge of the activation energy for surface migration on sputtered Si(111) and knowledge of the concentration of surface diffusers, i.e., so that one may use Eq. (2). Unfortunately, these values are not known. However, we do find that the temperature dependence of the parallel mode ripple wave vector extrapolated to $t=0$, $q_{app}(0)$, can be written in the form of Eq. (3) with an activation energy $E = 1.7 \pm 0.1 \text{ eV}$; a fit is shown in Fig. 5. This value is comparable to the sum of adatom migration energy and formation energy found in the literature,³⁴ but as discussed above, a definitive interpretation is premature. When performing the fit to Eq. (3), the value for B_0 is found to be $B_0 = 2.51 \times 10^{-18} \text{ eV cm}^4/\text{s}$. We may now perform a consistency check; we use Eq. (3) to estimate B at $T = 733 \text{ °C}$, and find it equal to $8.83 \times 10^{-26} \text{ cm}^4/\text{s}$. This value is close to the value found by analyzing R_q vs q shown

above. A final consistency check is to make a “back of the envelope” using $D_0 \sim 10^{-1} \text{ cm}^2/\text{s}$, $\gamma = 7.69 \times 10^{14} \text{ eV/cm}^2$,³⁵ and $\Omega = 2.0 \times 10^{-23} \text{ cm}^3$, to extract a value for ν_0 of $7.31 \times 10^{13} \text{ cm}^{-2}$. This value is of order 10% of the number of surface sites on Si(111), and in the athermal mobile species creation model would correspond to the surface concentration of diffusers. There are, of course, huge uncertainties with this estimate, but at least the estimate is neither greater than one, nor smaller than the thermal concentration of surface diffusers.

We have also used our $t=0$ extrapolation to measure the initial roughness spectrum $h_q(0)$. In general, we find reasonable measures for this quantity. For example, for parallel mode ripples formed at 733 °C, we obtain $h_q(0) = 0.287 \pm 0.041 \text{ nm}$ for $q \in [0.0077, 0.0131] \text{ nm}^{-1}$, a value comparable to the step height ($=0.314 \text{ nm}$) on Si(111).

B. Ripple coarsening with ion fluence

The observation of ripple coarsening is interesting because it is predicted by neither the linear Bradley-Harper theory⁶ nor the nonlinear extensions of BH theory.⁷ Coarsening of a characteristic length associated with roughening has previously been observed during low energy sputtering, although not usually in the context of ripple formation, and, in general, the characteristic lengths followed a power law.³⁶ In contrast, our empirical exponential decay form, Eq. (8), could always be used to describe coarsening. To understand this phenomenon in more detail, we have studied the applicability of kinetic Monte Carlo simulation to model ripple formation. This work is reported in detail elsewhere.²⁰ The simulation model described the surface as crystalline (i.e., as not amorphized during ion bombardment), as morphologically relaxed via surface diffusion, and as sputtered away via the Sigmund mechanism in which the probability of sputtering at a point on the surface is proportional to the energy deposited there. The primary conclusion of this work was that this description of the surface during sputtering is a “minimal model” sufficient to lead to ripple formation, coarsening, and indeed, the formation of transient ripple topographies. A natural consequence of this model is that step-edge dynamics play an important role in ripple formation and coarsening, which we discuss here.

Step-edge dynamics refers to the physics of fluctuation and interaction between discrete step edges found on crystal surfaces. Such interactions may be elastic or entropic. Of particular relevance in the evolution of unidirectional ripple structures is *terrace pinch-off*,³⁷ in which the pairs of opposing steps at the ripple peaks and valleys fluctuate into each other and locally annihilate (see Fig. 10). Once this occurs, a region of very high step curvature is created that evaporates very quickly, leading to the formation of terraces on the ripple peaks and in the valleys.³⁸ Thus if terrace pinch-off is present, there is a minimum terrace width at the ripple peak and valley that can be accommodated by the surface morphology. Because continued exponential growth of the ripple amplitude as predicted by the linear BH theory would lead to ripple peak terraces that approach zero width, terrace pinch-off is a short-circuit amplitude saturating mechanism.

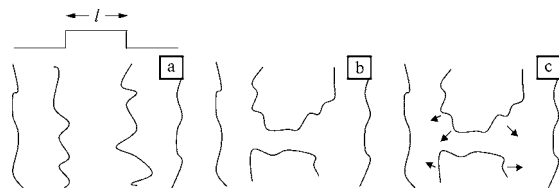


FIG. 10. Cartoon of surface relaxation due to terrace pinch-off. (a) An uppermost terrace has a width l and the steps at its edges are fluctuating in position. (b) Opposing steps eventually coalesce, and (c) increased line tension results in terrace dissolution.

In order to test for the presence of step-edge dynamics at the peaks and valleys of a sputter ripple feature with wave number q , we first approximate the surface profile $h(x)$ as a one-dimensional sinusoid with amplitude $H(t)$, i.e., $h(x) = H(t)\cos(xq^*)$ and then discretize this sinusoid as comprised of monoatomic-height steps [of height $s=0.314$ nm for Si(111)] and appropriately varying terrace widths. In this discrete step model of the ripple, the value of the topmost terrace width l , provided $l \ll \lambda$, is,

$$l = \sqrt{8s/Hq^2}. \quad (9)$$

For parallel mode ripples on Si(111), we have tracked the topmost terrace width of the apparent wave mode and find that for each sample this value initially decreases with sputtering time and then saturates to a value we denote by l_c , as shown in Fig. 11. This nonzero l_c implies that step-edge dynamics may indeed be active. In addition, we see an increase in l_c from ~ 60 to ~ 75 nm from 717 to 750 °C, consistent with a presence of a thermally activated process such as pinch-off. Similar behavior has been previously observed in the amplitude saturation of Si(001),¹⁴ the contrast being that for Si(001) no ripple coarsening was seen.

We were motivated by evidence of amplitude saturation and a critical terrace width to construct a toy model of the surface evolution in which the surface topography initially consisted of many Fourier components h_q of the same (small) amplitude H_0 . Each wave mode was allowed to grow

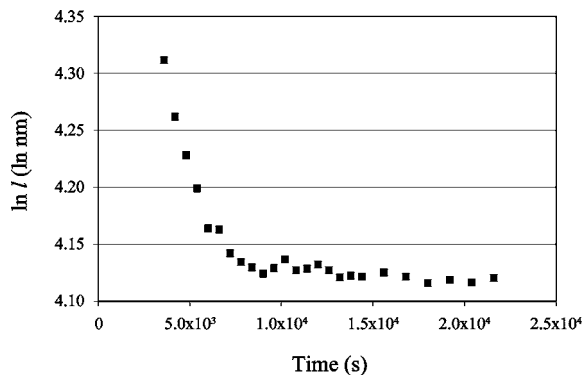


FIG. 11. Evolution of the uppermost terrace width $l(=\sqrt{8s/Hq^2})$ with sputtering time; $T=717$ °C, $f=0.75$ mA/cm². The uppermost terrace width of this sample stabilized at approximately 62 nm.

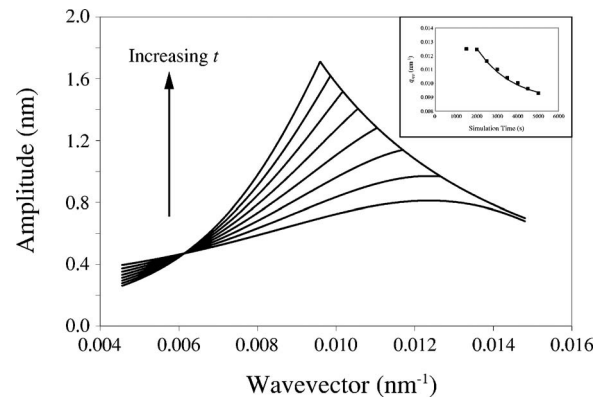


FIG. 12. Results of toy model for amplitude saturation discussed in the text. Here we illustrate the Fourier wave mode amplitude h_q vs q , using A , B , and C equal to -8.0×10^{-14} cm²/s, 2.64×10^{-24} cm⁴/s, and -2.6×10^{-4} 1/s, respectively, and $l_c=125$ nm. The data displays a trend that the apparent ripple wavelength coarsens with sputtering time. The inset shows that coarsening is well-described by an offset exponential decay (line), qualitatively in agreement with experiment (Ref. 39).

exponentially [cf. Eq. (4)] according to linear BH theory⁶ using experimental values for the roughening and relaxation prefactors A, B . However, when the uppermost terrace width l of a particular wave mode reached a critical terrace width l_c , the wave mode ceased to grow and its amplitude remained constant. Terrace pinch-off was the mechanism used to explain amplitude saturation.

Generically, at early times, the model looks similar to the BH form, i.e., exhibiting a time-independent maximally unstable wave mode. However, when the initially most unstable wave mode saturates, the apparent wavelength shifts to smaller values of q , values for which the corresponding amplitude may be greater, as shown in Fig. 12. The results from the numerical simulation are illustrated as a plot of h_q vs q for different simulation time (Fig. 12), and show an exponential decay in wave vector. Qualitatively, these results are similar to the experimental observation of coarsening. However, plugging realistic values of H_0 , R_q , and s into the model yields a coarsening rate that is about ten times faster than seen in experiment. This is perhaps not surprising considering that by truncating the short wavelength features, we are artificially accelerating the coarsening process.

VI. CONCLUSIONS

This paper describes a study of the morphological evolution of ion sputter induced ripple and dot formation on Si(111). Real time *in situ* LiSSp measurements as well as AFM allowed us to probe morphologies over a wide region of parameter space, including variations in sample temperature, ion flux, ion fluence, and ion energy. Our data show that in the low fluence regime, ripple growth initially proceeds exponentially, in accordance with the linear BH theory. Moreover, we found that it was possible to extract realistic

and self-consistent values for the roughening and relaxation terms described in this theory, and the activation energy for surface mass transport is reasonable. However, we also observed two phenomena that are not predicted by BH theory, dot formation/ripple rotation and ripple coarsening, which occur on this system over a wide range of sample temperature and ion fluence. Ripple coarsening is potentially described by consideration of discrete surface step dynamics at the peaks and valleys of the ripples. Perhaps most usefully, we were able to pinpoint regions in parameter space in which we are able to consistently produce highly ordered features within a certain range of lengthscales, and thus this study should assist in expanding the variety and morphological

control of self-organized nanostructures made with ion beam etching.

ACKNOWLEDGMENTS

We thank M. Makeev for making available his numerical integration code and J. Erickson for providing computing facilities. We gratefully acknowledge the generosity of K. Stebe for allowing us to use her AFM and M. J. Aziz, W. L. Chan, and E. Chason for useful discussions. This work was supported by the US Department of Energy under award number DE-FG02-01ER45942.

-
- ¹P. Haymann and J.-J. Trillat, C. R. Acad. Sci. URSS **248**, 2472 (1959).
- ²R. L. Cunningham, P. Haymann, C. Lecomte, W. J. Moore, and J. J. Trillat, J. Appl. Phys. **31**, 839 (1960).
- ³M. Navez, C. Sella, and D. Chaperot, C. R. Acad. Sci. URSS **254**, 240 (1962).
- ⁴F. Vasiliu, I. A. Teodorescu, and F. Glodeanu, J. Mater. Sci. **10**, 399 (1975).
- ⁵P. Sigmund, J. Mater. Sci. **8**, 1545 (1973).
- ⁶R. M. Bradley and J. M. E. Harper, J. Vac. Sci. Technol. A **6**, 2390 (1988).
- ⁷M. Makeev, R. Cuerno, and A. -L. Barabasi, Nucl. Instrum. Methods Phys. Res. B **197**, 185 (2002).
- ⁸E. Chason, T. M. Mayer, B. K. Kellerman, D. T. McIlroy, and A. J. Howard, Phys. Rev. Lett. **72**, 3040 (1994).
- ⁹W. L. Chan, N. Pavenayotin, and E. Chason, Phys. Rev. B **69**, 245413 (2004).
- ¹⁰J. Erlebacher, M. J. Aziz, E. Chason, M. B. Sinclair, and J. A. Floro, Phys. Rev. Lett. **82**, 2330 (1999).
- ¹¹S. Facsko, T. Dekorsy, C. Koerdts, C. Trappe, H. Kurz, A. Vogt, and H. L. Hartnagel, Science **285**, 1551 (1999).
- ¹²S. Facsko, T. Bobek, A. Stahl, and H. Kurz, Phys. Rev. B **69**, 153412 (2004).
- ¹³M. Castro, R. Cuerno, L. Vazquez, and R. Gago, Phys. Rev. Lett. **94**, 016102 (2005).
- ¹⁴J. Erlebacher, M. J. Aziz, E. Chason, M. B. Sinclair, and J. A. Floro, J. Vac. Sci. Technol. A **18**, 115 (2000).
- ¹⁵R. Cuerno and A.-L. Barabasi, Phys. Rev. Lett. **74**, 4746 (1995); M. A. Makeev and A.-L. Barabasi, Appl. Phys. Lett. **71**, 2800 (1997); S. Park, B. Kahng, H. Jeong, and A.-L. Barabasi, Phys. Rev. Lett. **83**, 3486 (1999).
- ¹⁶Y. Kuramoto, *Chemical Oscillations Waves and Turbulence* (Springer, Berlin, 1984); G. I. Sivashinsky, Acta Astronaut. **6**, 569 (1977).
- ¹⁷I. Koponen, M. Hautala, and O.-P. Sievanen, Phys. Rev. Lett. **78**, 2612 (1997).
- ¹⁸A. K. Hartmann and R. Kree, Phys. Rev. B **65**, 193403 (2002).
- ¹⁹M. Stepanova and S. K. Dew, Appl. Phys. Lett. **84**, 1374 (2004).
- ²⁰A.-D. Brown, J. Erlebacher, W.-L. Chan, and E. Chason, Phys. Rev. Lett. **95**, 056101 (2005).
- ²¹M. A. Makeev and A.-L. Barabasi, Appl. Phys. Lett. **71**, 2800 (1997).
- ²²F. Frost, A. Schindler, and F. Bigl, Phys. Rev. Lett. **85**, 4116 (2000).
- ²³W. W. Mullins, J. Appl. Phys. **30**, 1 (1959); C. Herring, in *The Physics of Powder Metallurgy*, edited by W. E. Kingston (McGraw-Hill, New York, 1951), Chap. 8.
- ²⁴L. Csepregi, E. F. Kennedy, J. W. Mayer, and T. W. Sigmon, J. Appl. Phys. **49**, 3906 (1978).
- ²⁵E. Chason, M. B. Sinclair, J. A. Floro, J. A. Hunter, and R. Q. Hwang, Appl. Phys. Lett. **72**, 3276 (1998).
- ²⁶J. M. Elson, Phys. Rev. B **30**, 5460 (1984).
- ²⁷In all instances we find that the parallel ripple peak to valley amplitude is less than 5 nm; this value can exceed 100 nm for perpendicular ripple morphologies.
- ²⁸W. L. Chan (personal communication).
- ²⁹J. D. Erlebacher, Ph.D. thesis, Harvard University, 1998.
- ³⁰S. Hazra, T. K. Chini, M. K. Sanyal, J. Grenzer, and U. Pietsch, Phys. Rev. B **70**, 121307(R) (2004).
- ³¹R. A. Enrique and P. Bellon, Phys. Rev. Lett. **84**, 2885 (2000).
- ³²A.-D. Brown and J. Erlebacher (unpublished).
- ³³The values for the ion range=2.8 nm, the longitudinal straggle =1.6 nm, and lateral straggle=0.9 nm were estimated using SRIM 2003 by projecting the longitudinal range into the direction of the ion beam and by separating the longitudinal straggle into components parallel to and perpendicular to the ion beam direction.
- ³⁴A. Pimpinelli, J. Villain, D. E. Wolf, J. J. Metois, J. C. Heyraud, I. Elkinani, and G. Uimin, Surf. Sci. **295**, 143 (1993).
- ³⁵J. Jaccodine, J. Electrochem. Soc. **110**, 524 (1963).
- ³⁶M. V. Ramana Murty, T. Curcic, A. Judy, B. H. Cooper, A. R. Woll, J. D. Brock, S. Kycia, and R. L. Headrick, Phys. Rev. Lett. **80**, 4713 (1998).
- ³⁷J. D. Erlebacher and M. J. Aziz, Surf. Sci. **374**, 427 (1997).
- ³⁸J. Villain, J. Phys. (Paris) **49**, 257 (1988).
- ³⁹Fourier modes at small q decrease in amplitude due to the effect of the negative value of C .